J|A|C|S
ARTICLES
Published on Web 02/19/2004

Polymorphism in $NaSbO_3$: Structure and Bonding in Metal Oxides

Hiroshi Mizoguchi,[§] Patrick M. Woodward,*[,§] Song-Ho Byeon,[†,||] and John B. Parise[†,‡]

Contribution from the Department of Chemistry, Ohio State University, Columbus, Ohio 43210-1185, Department of Geosciences and Mineral Physics Institute, State University of New York, Stony Brook, New York 11794-2100, and Department of Chemistry, State University of New York, Stony Brook, New York 11794-3400

Received September 5, 2003; E-mail: woodward@chemistry.ohio-state.edu

Abstract: A new polymorph of $NaSbO_3$ has been synthesized at 10.5 GPa and 1150 °C in a uniaxial split sphere anvil type press (USSA-2000) and recovered back to ambient conditions. The high-pressure form of $NaSbO_3$ adopts an orthorhombically distorted perovskite structure, isostructural with $CaTiO_3$, $GdFeO_3$, and $NaTaO_3$. The space group is *Pnma*, and the unit cell dimensions are $a = 5.43835(6)$ Å, $b = 7.66195(8)$ Å, $c = 5.38201(5)$ Å. It is a white insulator with an optical band gap of 3.4 eV. This compound represents the first ternary perovskite prepared containing Sb^{5+} on the octahedral site. The octahedral tilting distortion in this compound is much larger than expected from ionic radii considerations. The distortion is driven by a second-order Jahn−Teller distortion originating on oxygen that can be traced back to strong Sb−O covalent bonding. A conflict arises between the strong covalent bonding interactions at oxygen that favor a large octahedral tilting distortion and the repulsive Na−O interactions that oppose excessive octahedral tilting. This conflict destabilizes the perovskite topology, thereby stabilizing the ilmenite polymorph under ambient conditions. Analysis of ionic and covalent bonding explains why $ASbO_3$ and $ABiO_3$ compositions frequently adopt structures that violate Pauling's rules.

1. Introduction

The perovskite structure is perhaps the most frequently encountered structure type among ternary and quarternary oxides. Members of the perovskite family have numerous properties that find technological application, such as ferroelectricity, piezoelectricity, superconductivity, colossal magnetoresistance, catalysis, and ionic conductivity (including O^{2-}, H^+, and Li^+) among others. Consequently, perovskites have been an integral part of oxide materials chemistry research for over five decades now. Oxide perovskites ideally have AMO_3 stoichiometry with a structure that consists of a three-dimensional framework of corner sharing MO_6 octahedra. In the ideal cubic structure the A cation sits on a dodecahedral site surrounded by 12 oxide ions. Symmetry-lowering distortions are common in cases where the sizes of the two cations are not perfectly matched. The size match of the two cations can be reliably estimated from the tolerance factor, $\tau = (r_A + r_O)/\{\sqrt{2}(r_M + r_O)\}$,[1] which adopts a value of unity if the $M-O$ and $A-O$ bond distances are perfectly matched. Perovskites are particularly common in cases where the octahedral cation, M, is a transition metal ion (i.e., $CaTiO_3$, $LaCoO_3$, $SrRuO_3$, $NaTaO_3$, $CaMnO_3$, etc.). The perovskite structure is also observed for compounds where M is a main group ion (i.e., $LaAlO_3$, $LaGaO_3$, $BaSnO_3$, $BaPbO_3$, etc.). However, in such compositions the stability of the perovskite structure apparently decreases as the covalency of the $M-O$ interaction increases. Thus, perovskites where Si^{4+} and Ge^{4+} occupy the octahedral site have to be made at high pressure, and in some cases, particularly if $M = Si^{4+}$, they cannot be stabilized upon the release of pressure. Despite the intrinsic instability of these phases, geologists have a keen interest in silicate perovskites because $MgSiO_3$ and substituted variants this compound are generally accepted to be the most abundant minerals in the earth's mantle.[2]

Interestingly there are no reports of ternary perovskites containing Sb^{5+}, despite the fact that this ion prefers octahedral coordination and has an electronegativity that is comparable to that of Ge^{4+}. There is a similar absence of the perovskite structure among ternary oxides of Bi^{5+}. However, the instability of the perovskite structure among ternary oxides of pentavalent antimony and bismuth is not a trait shared by oxides of their d^0 transition metal counterparts, Nb^{5+} and Ta^{5+}. The structures of AMO_3 compositions ($A = Na^+$, K^+; $M = Sb^{5+}$, Bi^{5+}, Nb^{5+}, Ta^{5+}) are summarized in Table 1 and illustrated in Figure 1. For the antimonates and bismuthates, the ilmenite and cubic $KSbO_3$-type structures, both of which possess edge-sharing octahedra, are seen to be the most prominent. The preference

§ The Ohio State University, Department of Chemistry.
† Department of Geosciences and Mineral Physics Institute, State University of New York.
‡ Department of Chemistry, State University of New York.
|| On leave from College of Environment and Applied Chemistry, Kyung Hee University, Kyung Ki 449-701, Korea.

(1) Goldschmidt, V. M. *Akad. Oslo I. Mat.-Nat.* **1926**, *2*, 7.
(2) Shim, S. H.; Duffy, T. S.; Shen, G. Y. *Science* **2001**, *293*, 2437.

Table 1. Structural Details for $A^+M^{5+}O_3$-type Oxides at Room Temperature

	τ[c]	structure type	space group	M^{5+}–O distances (Å)	average M–O–M angle (deg)	A bond valence sum[a]	M bond valence sum[a]
$NaNbO_3$[6]	0.97	distorted perovskite	*Pbcm*	1.88, 1.88, 1.94, 2.02, 2.10, 2.11	158.1	1.01	5.02
$NaTaO_3$[7]	0.97	distorted perovskite	*Pnma*	2 × 1.98, 2 × 1.98 2 × 1.98	159.2	1.04	5.13
$NaSbO_3$[8]	0.99	ilmenite	$R\bar{3}$	3 × 1.98 3 × 2.01	100.3	1.17	5.23
$NaBiO_3$[9]	0.92	ilmenite	$R\bar{3}$	3 × 2.09 3 × 2.14	101.5	1.10	5.17
$KNbO_3$[10]	1.06	distorted perovskite	*Amm*2	2 × 1.87, 2 × 2.00 2 × 2.17	171.1	1.81	4.80
$KTaO_3$[11]	1.06	cubic perovskite	$Pm\bar{3}m$	6 × 1.99	180	1.87	4.91
$KSbO_3$[12]	1.08	cubic $KSbO_3$	$Pn\bar{3}$	2 × 1.87, 2 × 2.04 2 × 2.11	97.6 129.9	K(1): 1.74 K(2): 1.00[b]	4.70
$KSbO_3$[12]	1.08	ilmenite	$R\bar{3}$	3 × 1.96 3 × 2.10	99.9	1.54	4.86
$KBiO_3$[13]	1.00	cubic $KSbO_3$	$Pn\bar{3}$	2 × 2.08 2 × 2.11 2 × 2.12	98.2 128.0	0.87[b]	5.34

[a] Bond valence parameters used were as follows R_0(Na−O) = 1.803, R_0(Nb−O) = 1.911, R_0(Ta−O) = 1.920, R_0(Sb−O) = 1.942, and R_0(K−O) = 2.132. The calculations were done with the program VALENCE.[14] The value of R_0(Bi−O) = 2.06 was taken from Brese and O'Keeffe.[15] [b] These compounds generally contain crystallographic water. The low bond valence sums for K^+ in these compounds could arise from coordination of H_2O to potassium. [c] The tolerance factor is represented by τ.

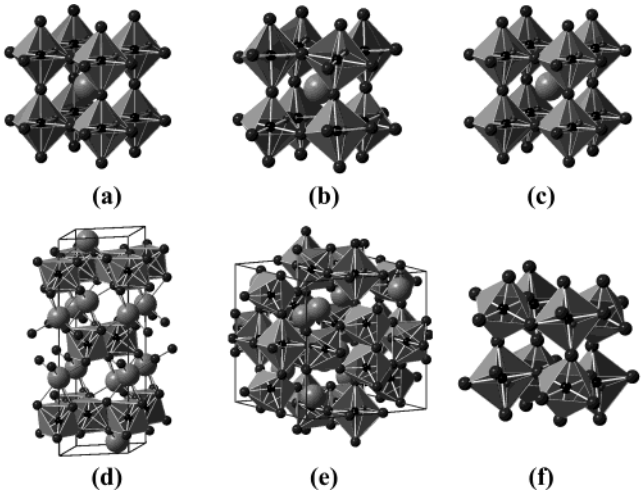

Figure 1. Crystal structures of (a) $BaSnO_3$ (cubic perovskite), (b) $NaTaO_3$ (*Pnma* perovskite, distorted by octahedral tilting), (c) $KNbO_3$ (*Amm*2 perovskite, distorted by Nb^{5+} displacements toward the octahedral edges) (d) $NaSbO_3$ (ilmenite), (e) cubic $KSbO_3$, and (f) TeO_3 ($R\bar{3}c$ perovskite, distorted by octahedral tilting).

for structures containing edge-sharing octahedra over the corner-sharing connectivity of the perovskite structure is a clear violation of Pauling's third rule for determining the structures of ionic compounds.[3] It is particularly striking that $NaSbO_3$ does not adopt the perovskite structure despite a tolerance factor that is very close to unity.

The differences in the structural tendencies and physical properties of these seemingly similar ions provide an interesting area for the study of bonding in inorganic solids. Previously Blasse[4] as well as Goodenough and Kafalas[5] examined the different crystal chemistry of these ions in general, and $NaMO_3$ compositions in particular. Blasse suggested that M $(n - 1)$d−O 2p π-bonding is responsible for stabilizing the perovskite topology for $NaTaO_3$ and $NaNbO_3$. He also pointed out that an asymmetrical cation distribution about the oxide sites favors anion polarization effects, which tilts the balance in favor of edge-sharing octahedra in the case of $NaSbO_3$. Goodenough and Kafalas also stressed the role of M−O π-bonding in stabilizing linear $M-O-M$ bonds, and asserted that in the absence of π-bonding interactions (i.e. with Sb^{5+} and Bi^{5+}) strong covalency favors edge sharing and ∼90° $M-O-M$ bond angles.

There are a number of nonperovskite AMO_3 phases that convert to perovskite at high pressure. In addition to the aforementioned $MgSiO_3$, the germanates $CaGeO_3$[16] and $SrGeO_3$[17] can be prepared under high-pressure−high-temperature conditions. Consequently, there is reason to believe that ternary perovskites containing Sb^{5+} and Bi^{5+} might be prepared by the same route. Previously Hong et al. subjected the ilmenite phases $KSbO_3$ and $NaSbO_3$ as well as the defect pyrochlore phase $AgSbO_3$ to high-pressure−high-temperature conditions in a belt-type apparatus.[18] They were able to transform the ilmenite form of $KSbO_3$ to the cubic polymorph (see Figure 1e) at a pressure in excess of 2 GPa and a temperature of 700 °C. However, under these conditions $NaSbO_3$ and $AgSbO_3$ retained their ambient pressure structures, ilmenite and defect pyrochlore, respectively. We felt it would be interesting to investigate the response of these two compounds to treatment at higher pressures and temperatures to see if perovskite phases could be obtained. While we have not yet been able to obtain a perovskite polymorph of $AgSbO_3$, we have succeeded in converting $NaSbO_3$ from ilmenite structure to perovskite and in recovering this phase to ambient conditions.

(3) Pauling, L. *J. Am. Chem. Soc.* **1929**, *51*, 1010.
(4) Blasse, G. *J. Inorg. Nucl. Chem.* **1964**, *26*, 1191.
(5) Goodenough, J. B.; Kafalas, J. A. *J. Solid State Chem.* **1973**, *6*, 493.
(6) Hewat, A. W. *Ferroelectrics* **1974**, *7*, 83.
(7) Kennedy, B. J.; Prodjosantoso, A. K.; Howard, C. J. *J. Phys. Condens. Matter* **1999**, *11*, 6319.
(8) Wang, B.; Chen, S. C.; Greenblatt, M. *J. Solid State Chem.* **1994**, *108*, 184.
(9) Kumada, N.; Kinomura, N.; Sleight, A. W. *Mater. Res. Bull.* **2001**, *35*, 2397.
(10) Hewat, A. W. *J. Phys. C: Solid State Phys.* **1973**, *6*, 2559.
(11) Wyckoff, R. W. G. *Crystal Structures*; Interscience: New York, 1968; Vol. 2.
(12) Spiegelberg, P. *Ark. Kemi Miner. Geol.* **1940**, *14*, 1.
(13) Kodialam, S.; Korthius, V. C.; Hoffmann, R. D.; Sleight, A. W. *Mater. Res. Bull.* **1992**, *27*, 1379.
(14) Brown, I. D. *J. Appl. Crystallogr.* **1996**, *29*, 479.
(15) Brese, R. E.; O'Keeffe, M. *Acta Crystallogr., Sect. B* **1991**, *47*, 192.
(16) Ross, N. L.; Akaogi, M.; Navrotsky, A.; Susaki, J.-I.; McMillan, P. F. *J. Geophys. Res.* **1986**, *91*, 4685.
(17) Grzechnik, A.; McMillan, P. F.; Chamberlin, R.; Hubert, H.; Chizmeshya, A. V. G. *Eur. J. Solid State Inorg. Chem.* **1997**, *34*, 269.
(18) Hong, H. Y−P.; Kafalas, J. A.; Goodenough, J. B. *J. Solid State Chem.* **1974**, *9*, 345.

This paper describes the high-pressure−high-temperature synthesis of the perovskite polymorph of $NaSbO_3$, the first example of a ternary perovskite containing Sb^{5+}. The crystal and electronic structure of this compound are compared with a number of related phases, including the ilmenite polymorph of $NaSbO_3$ and the perovskite form of $NaTaO_3$. The new experimental results coupled with the advances in the speed and accuracy of electronic structure calculations allow for a level of comparison that was not previously available. Our analysis shows that the structural preferences of these compounds are dictated in large part by the bonding preferences of the oxide anions. Distortions from the cubic perovskite structure to the orthorhombic perovskite structure and finally to the ilmenite structure are driven primarily by a second-order Jahn−Teller distortion about the oxide ion. Ionic interactions between the larger *A*-site cations (i.e. Na^+, K^+) and oxygen also play a pivotal role in determining the relative stability of competing phases. The comparisons presented in this contribution offer insight into the relative stability of competing phases, structure−bonding-property relationships, and the prospects for preparing additional perovskites containing main group ions in high oxidation states. The formation and behavior of these compounds under pressure has important implications both for materials chemistry and for geologic studies of the earth's interior.

2. Experimental Section

2.1. Synthesis. $NaSbO_3$ in its ilmenite form was synthesized by conventional solid-state reaction from $NaCO_3$ (anhydrous, Fisher, ACS, 99.5%) and Sb_2O_3 (Cerac, 99.9%). The mixture was heated to 1000 °C for 10 h in air. The ilmenite product was then thoroughly reground and sealed in a Au capsule with an inner diameter of 3.2 mm and a wall thickness of 0.1 mm. High-pressure−high temperature (HPHT) reactions were tried at several conditions between 10−14 GPa and 1000−1200 °C with the 2000-ton Uniaxial Split Sphere high-pressure apparatus (USSA 2000).[19] The final polycrystalline sample was obtained from high-pressure treatment at 10.5 GPa and 1150 °C for 4 h, followed by temperature quenching and slow decompression. The sample was recovered from the Au capsule as a dense pellet with a volume of roughly 50 mm^3. Details of the cell assembly along with the temperature and the pressure calibrations are described in the literature.[20,21] Further details regarding high-pressure−high-temperature synthesis of perovskites can also be found in the literature.[22,23] The formation of a new polymorph of $NaSbO_3$ was initially confirmed from an X-ray powder diffraction pattern, taken on the sample pellet after recovery from HPHT reaction with a general area detector diffraction system (GADDS). The cation stoichiometry was confirmed by X-ray energy dispersive spectroscopy with a JEOL, JSM-820 scanning electron microscope, equipped with an Oxford eXL analyzer.

2.2. X-ray Powder Diffraction and Diffuse Reflectance Spectroscopy. X-ray powder diffraction data suitable for structure refinement were collected in Debye-Sherrer mode with a Bruker D8 X-ray powder diffractometer (40 kV−50 mA, sealed Cu X-ray tube) equipped with an incident beam Ge 111 monochromator, which selects only Cu $K\alpha_1$ radiation ($\lambda = 1.5406$ Å), and a Braun linear position sensitive detector. The powder sample was sealed in 0.2 mm diameter glass capillary. The capillary was rotated continuously about its long axis during data collection. Structure refinements were performed with the Rietveld method[24] as implemented in the TOPAS software package.[25] UV−visible diffuse reflectance data were collected over the spectral range 240−1100 nm with a Perkin-Elmer Lambda 20 scanning double-beam spectrometer, equipped with a 50 mm Labsphere integrating sphere. MgO was used as a reference. The Kubelka−Munk function was used to transform the data into absorbance.

Table 2. Potential and Polarization Parameters Utilized for the Lattice Energy Calculations (GULP)

	A (eV)	*ρ* (Å)	*C* (eV/Å^6)	q_{core} (e$^-$)	q_{shell} (e$^-$)	*k* (eV/Å^2)
Na^+-O^{2-}	1271.504	0.3000	0.0	1.000	0.000	0
$Sb^{5+}-O^{2-}$	18752.22	0.2219	0.0	2.105	2.895	101.2
$Nb^{5+}-O^{2-}$	3023.184	0.3000	0.0	5.000	0.000	0
$Ta^{5+}-O^{2-}$	2927.94	0.3000	0.0	5.000	0.000	0
$O^{2-}-O^{2-}$	25.410	0.6937	32.32	0.513	−2.513	20.53

2.3. Lattice Energy Calculations. Lattice energy calculations were carried out with the General Utility Lattice Program (GULP).[26] GULP calculates the lattice energy for a structure by considering the electrostatic interactions that hold an ionic crystal together as well as the short-range repulsive interactions that prevent ion−ion distances from becoming too short. Forces are assumed to be of the two-body type. The interatomic interactions are divided into long-range Columbic and short-range forces. The short-range interactions are modeled with a Buckingham potential, shown below:

$$A_{ij}\exp(-r_{ij}/\rho_{ij}) - C_{ij}/r_{ij}^6$$

where A_{ij}, ρ_{ij}, and C_{ij} are empirical parameters used to describe the interaction between ions *i* and *j*, and r_{ij} is the distance between the ions. Potential and polarization parameters determined by Battle et al.[27] and Woodley et al.[28] were adopted for this study. The parameters for $Ta^{5+}-O^{2-}$ were obtained with the relaxed fitting procedure[29] implemented in GULP. The Ta^{5+} parameters were optimized based on the experimental structure of $KTaO_3$ along with the K^+ and O^{2-} parameters previously determined by Bush, et al.[29b] The full list of empirical parameters used in this study are shown in Table 2. A core−shell model was used in the calculations to model the polarization of oxygen.[30] In this model each ion is divided into a core (nucleus plus core electrons) and a massless shell (valence electrons). The position of the shell is coupled to its corresponding core by a harmonic spring. The magnitude of the spring constant provides a parameter for varying the polarizability of a given ion.

To evaluate the relationship between covalent bonding and crystal structure in a more rigorous manner we also employed total electronic energy calculations to evaluate the stability and preferred geometry of competing crystal structures. The density functional theory (DFT) calculations were carried out with the Cambridge Serial Total Energy Package (CASTEP) code,[31] which uses plane wave basis sets for the valence electrons. Pseudopotential theory is utilized to include the influence of the core electrons. The exchange-correlation potential of the electron gas was treated with the generalized gradient-corrected approximation (GGA).

2.4. Electronic Band Structure Calculations. Band structure calculations were performed with the linear muffin-tin orbital (LMTO) method with the atomic sphere approximation (ASA) including the

(19) Liebermann, R. C.; Wang, Y. *High-Pressure Research: Application to Earth and Planery Sciences*; Terrapub: Tokyo, 1992.
(20) Gwanmesia, G. D.; Li, B.; Liebermann, R. C. *PAGEOPH* **1993**, *141*, 467.
(21) Leinenweber, K.; Parise, J. B. *J. Solid State Chem.* **1995**, *114*, 277.
(22) Park, J.-H.; Woodward, P. M.; Parise, J. B. *Chem. Mater.* **1998**, *10*, 3092.
(23) Byeon, S.; Lufaso, M. W.; Parise, J. B.; Woodward, P. M.; Hansen, T. *Chem. Mater.* **2003**, *15*, 3798.
(24) Young, R. A. *The Rietveld Method*; Oxford: London, 1995.
(25) Cheary, R. W.; Coelho, A. A. *J. Appl. Crystallogr.* **1992**, *25*, 109.
(26) Gale, J. D. *J. Chem. Soc., Faraday Trans.* **1997**, *93*, 629.
(27) Battle, P. D.; Bush, T. S.; Catlow, C. R. A. *J. Am. Chem. Soc.* **1995**, *117*, 6292.
(28) Woodley, S. M.; Battle, P. D.; Gale, J. D.; Catlow, C. R. A. *Phys. Chem. Chem. Phys.* **1999**, *1*, 2535.
(29) (a) Gale, J. D. *Philos. Mag. B* **1996**, *73*, 3. (b) Bush, T. S.; Gale, J. D.; Catlow, C. R. A.; Battle, P. D. *J. Mater. Chem.* **1994**, *4*, 831.
(30) Dick, B. G.; Overhauser, A. W. *Phys. Rev.* **1958**, *112*, 90.
(31) Payne, M. C.; Teter, M. P.; Allen, D. C.; Arias, T. A.; Joannopoulos, J. D. *Rev. Mod. Phys.* **1992**, *64*, 1045.

Table 3. Rietveld Refinement Details for the Perovskite Polymorph of $NaSbO_3$[a]

R_{wp}	11.83
R_{Bragg}	7.54
χ^2	1.85
2θ range (deg)	15−120
no. of reflections	190
no. of variables	28
space group	*Pnma* (no. 62)
a (Å)	5.43835(6)
b (Å)	7.66195(8)
c (Å)	5.38201(5)
volume (Å^3)	224.260(4)

[a] Further details regarding the data collection and analysis are given in section 2.2.

Table 4. Atomic Coordinates as Determined from the Rietveld Refinement of the Perovskite Polymorph of $NaSbO_3$

atom	Wyckoff site	x	y	z	U_{iso} (Å^2)
Na	4c	0.532(2)	1/4	0.511(4)	0.056(8)
Sb	4b	1/2	0	0	0.027(1)
O(1)	4c	0.977(4)	1/4	0.422(2)	0.008(4)[a]
O(2)	8d	0.294(2)	0.040(1)	0.712(2)	0.008(4)[a]

[a] The displacement parameters for the O(1) and O(2) sites were constrained to be equal.

combined correction (CC). The LMTO-ASA code used in these calculations was developed in Stuttgart by Andersen and co-workers.[32] k-space integrations employed the tetrahedron method using 105 irreducible k points within the Brillouin zone (BZ). In the case of $NaSbO_3$ (*Pnma*) the default value of irreducible k points within the BZ was used. The basis sets consisted of the valence s, p, and d orbitals of cations and the 2s and 2p orbitals of oxygen. The Perdew−Wang GGA exchange correlation was used.[33]

3. Results

3.1. Synthesis and Characterization. On the basis of X-ray powder diffraction analysis, we found that the perovskite form of $NaSbO_3$ forms as the dominant phase at 10 GPa and 1000 °C. Impurity phase(s) were found to be minimal in the sample prepared by treating the ilmenite polymorph of $NaSbO_3$ at 1150 °C and 10.5 GPa for 4 h. The high-pressure phase was stabilized by a temperature quench followed by slow release of the pressure. This procedure yielded a white powder. X-ray powder diffraction (XRPD) measurements confirmed the phase as a distorted perovskite. The symmetry is lowered from cubic to orthorhombic by an octahedral tilting distortion so that the high-pressure form of $NaSbO_3$ is isostructural with $NaTaO_3$ (shown in Figure 1b) and the mineral perovskite, $CaTiO_3$. The space group is *Pnma*. Unit cell dimensions and other details from the structure refinement are given in Table 3. Atomic coordinates are given in Table 4, while selected bond distances and angles are shown in Table 5. The refined XRPD pattern is shown in Figure 2. It should be noted that the density of perovskite form (5.706 g/cm^3) is considerably higher than that of ilmenite form (4.976 g/cm^3). This observation helps to explain the stabilization of perovskite phase at high pressures.

The diffuse reflectance spectra for the two polymorphs of $NaSbO_3$ along with spectra from some related phases are shown in Figure 3. The band gap of the perovskite form is considerably smaller than that of the ilmenite polymorph (3.4 eV vs ∼4.9 eV). Among compounds within the perovskite family $NaSbO_3$ has a band gap that is similar in magnitude to the cubic perovskites $KTaO_3$ (3.6 eV) and $BaSnO_3$ (3.1 eV), and much larger than the semimetallic $BaPbO_3$. However, the band gap of $NaSbO_3$ is noticeably smaller than the similarly distorted perovskites $NaTaO_3$ (4.0 eV), $SrSnO_3$ (4.1 eV), and $CaSnO_3$ (4.4 eV).

Table 5. Selected Bond Distances and Bond Angles from Refinement of the Perovskite Form of $NaSbO_3$

Bond Distances (Å)	
Na−O(8d)	2 × 2.33(2), 2 × 2.62(2), 2 × 2.70(1)
Na−O(4c)	2.35(2), 2.47(3), 3.06(3), 3.07(2)
Sb−O(8d)	2 × 1.94(1), 2 × 1.99(1)
Sb−O(4c)	2 × 1.965(2)
Bond Angles (°)	
O−Sb−O	88.7(6), 88.9(5), 89.0(1), 91.0(1), 91.1(5), 91.3(6)
Sb−O−Sb	154.2(6), 154.2(8)

3.2. Lattice Energy Calculations. Oxides are generally considered to be ionic compounds, and as such they are expected to be electrically insulating and mechanically brittle. Yet the conductivity and optical properties of compounds such as ReO_3, Na_xWO_3, $YBa_2Cu_3O_{7-x}$, and $BaPbO_3$ reminds us that the simple ionic picture is not appropriate for many oxides. In general the covalency of the metal−oxygen bonds will increase as the electronegativity and oxidation state of the metal cation increases, so that in oxides containing pentavalent metal cations, such as Sb^{5+}, Bi^{5+}, Nb^{5+}, and Ta^{5+}, both ionic and covalent interactions must be taken into account. In this study computational tools were utilized to evaluate the combined effects of ionic and covalent bonding from two different perspectives. Some measure of covalency can be introduced into lattice energy calculations by considering ion polarization effects, through the core−shell approach. Total energy calculations were also carried out with the DFT approach incorporated in the CASTEP software. These calculations explicitly take into account the energy of the valence electrons, and hence they treat covalent interactions in a much more rigorous manner. Yet they retain aspects of ionic energy by considering the effect of ion cores on the valence electrons and each other. The combined use of these two computational approaches gives an insightful picture of the structure−bonding relationships in NaMO$_3$ (M = Sb, Nb, Ta) compounds.

Figure 4 shows the calculated lattice energy for $NaSbO_3$, $NaNbO_3$, and $NaTaO_3$ in three structural configurations: cubic perovskite ($Pm\bar{3}m$), orthorhombic perovskite (*Pnma*), and ilmenite ($R\bar{3}$), as well as the total energy as calculated by CASTEP for each of these three structural modifications. Experimentally determined crystal structures were used where they were available, namely for the ilmenite modifications of $NaSbO_3$[8] and $NaNbO_3$,[34] and the orthorhombic perovskite forms of $NaSbO_3$ and $NaTaO_3$.[7] The cubic perovskite modifications for all three compounds, the *Pnma* orthorhombic perovskite structure of $NaNbO_3$ and the ilmenite structure of $NaTaO_3$, were obtained with the BFGS geometrical optimization feature of CASTEP. The CASTEP optimized perovskite structures possessed symmetric octahedra with M−O distances, 1.96 Å ($NaSbO_3$), 1.99 Å ($NaNbO_3$), 1.99 Å ($NaTaO_3$) and 1.99 Å (*Pnma* $NaNbO_3$), which are in very good agreement with the

(32) Andersen, O. K.; Jepsen, O. *Phys. Rev. Lett.* **1984**, *53*, 2571.
(33) Perdew, J. P.; Wang, Y. *Phys. Rev. B* **1986**, *33*, 8800.
(34) (a) Kinomura, N.; Kumada, N.; Muto, F. *Mater. Res. Bull.* **1984**, *19*, 299. (b) Kumada, N.; Kinomura, N.; Muto, F. *J. Ceram. Soc. Jpn.* **1990**, *98*, 384.

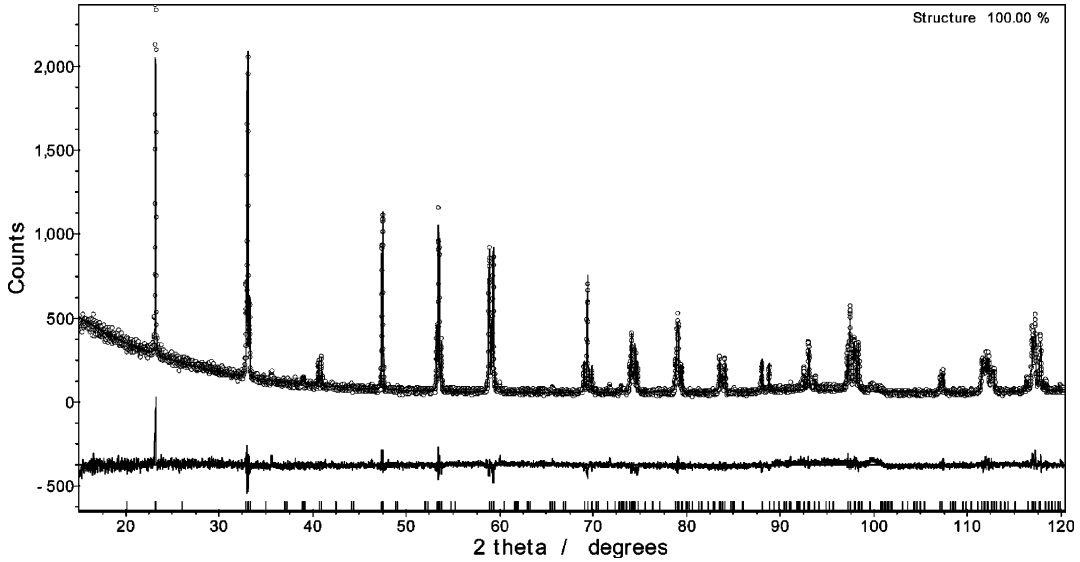

Figure 2. Observed X-ray powder diffraction pattern (points) for the $NaSbO_3$ sample obtained after high-pressure−high-temperature treatment, along with the calculated (gray curve) and difference (lower curve) patterns from the Rietveld refinement. Vertical bars denote the expected peak positions.

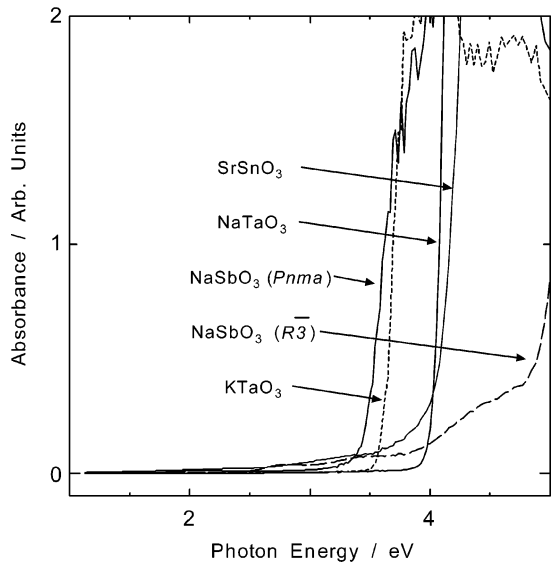

Figure 3. UV−visible diffuse reflectance data for perovskite $NaSbO_3$, ilmenite $NaSbO_3$, $SrSnO_3$, $NaTaO_3$, and $KTaO_3$.

distances that would be expected from ionic radii considerations,[35] 1.95 Å (Sb−O), 1.99 Å (Nb−O), and 1.99 Å (Ta−O). Ferroelectric displacements of Nb^{5+} ions in the perovskite forms of $NaNbO_3$ were not taken into account.

The filled circles in Figure 4 show the lattice energies as calculated by GULP in the absence of polarization, while the open circles show the lattice energy once polarization is permitted. In the absence of polarization the calculations suggest both compounds favor the cubic perovskite structure. The stabilization of the cubic perovskite structure is particularly pronounced if compared to the ilmenite structure. These results are perfectly consistent with Pauling's rules, as expected, since both Pauling's rules and the lattice energy calculations are predominantly based on electrostatic considerations. It is interesting to see what happens when polarization is included. The orthorhombic perovskite structure receives a modest gain in energy (0.2−0.6%), while the ilmenite structure gets a more significant gain in energy (3−4%), and polarization has no effect on the energy of the cubic perovskite structure. Once polarization has been included the GULP calculations suggest that all three structures have similar energies.

The polarization contribution or lack thereof can be understood once we recognize that the predominant polarization mechanism is polarization of the oxide electron cloud by the smaller and highly charged M^{5+} ions. In the cubic perovskite structure the $M-O-M$ bonds are linear, and the polarizing effects of the two cations cancel out. Hence, there is no additional stabilization due to polarization (in the dipole approximation). The ilmenite structure represents the other extreme. The edge-sharing octahedra give $M-O-M$ bond angles that approach 90° so that the electron cloud of the oxide anion is being pulled in a common direction by the two M^{5+} ions. The polarization effects in the orthorhombic perovskite structure are considerably smaller than those observed in ilmenite, but not completely negligible. A pictorial representation of the polarization effects in these two structures is shown in Figure 5. The black sphere shows the location of the oxygen core, while the pink sphere shows the centroid position of oxygen shell. In both structures the oxide shells are shifted in such a way as to move them closer to the neighboring M^{5+} ions, but the shift is clearly more pronounced for the ilmenite structure. The average oxygen core−shell distance is 0.15 Å (0.08 Å) for the orthorhombic perovskite form of $NaSbO_3$ ($NaNbO_3$) and 0.22 Å (0.21 Å) for the ilmenite form of $NaSbO_3$ ($NaNbO_3$). These calculations give a quantitative confirmation of the earlier ideas of Blasse.[4] It should be kept in mind that the GULP lattice energy calculations do not take into account the possibility of π-bonding. They merely tell us that stabilization arising from anion polarization effects will be nonexistent in the cubic perovskite structure and most favorable in the ilmenite structure. The polarization contribution in the orthorhombic *Pnma* perovskite structure will be intermediate, increasing as the degree of octahedral tilting increases.

The GULP calculations confirm that electrostatic interactions favor the cubic perovskite structure. They also show that polarization effects make an important contribution to the

(35) Shannon, R. D. *Acta Crystallogr., Sect. A* **1976**, *32*, 751.

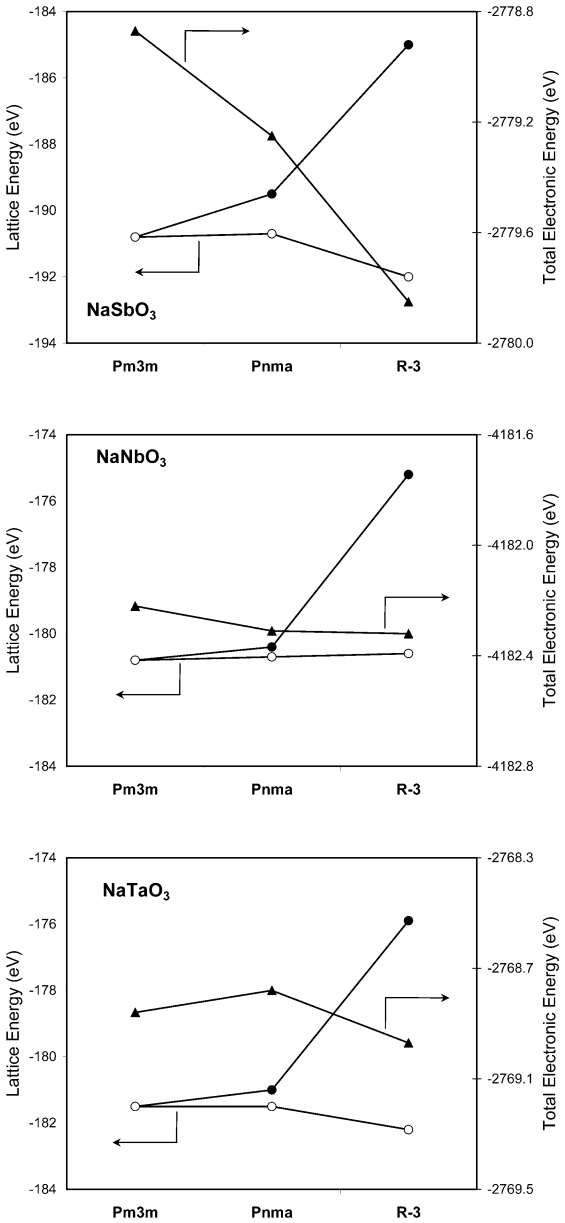

Figure 4. Lattice energy and relative total electronic energy for Na*M*O_3 compounds in three competing structural modifications. Open and filled circles show the lattice energy with and without polarization effects included, respectively. Triangles show the total electronic energy obtained by CASTEP. The vertical scales were chosen to maintain the same range for each of the three compounds.

stability of the ilmenite structure. If one interprets the calculations quantitatively, it appears that anion polarization effects effectively cancel out much of the stabilization of the cubic perovskite structure. Nonetheless, the lattice energy calculations do not explain the contrasting structural preferences of $NaSbO_3$ and Na*M*O_3 (*M* = Nb, Ta). To understand the different crystal chemistry of the Sb^{5+} and Nb^{5+}/Ta^{5+} ions it is necessary to explicitly consider orbital overlap and covalent bonding. To do so, energy calculations were carried out with CASTEP for each of the phases evaluated above with GULP. The results are also plotted in Figure 4. $NaSbO_3$ shows a pronounced trend toward increasing stability upon going from cubic perovskite through orthorhombic perovskite to ilmenite, while there is very little change in total energies of the competing structure types for $NaNbO_3$ and $NaTaO_3$. The reason for this trend can be understood in simple terms. First of all, we need to recognize the fact that Nb^{5+} and Ta^{5+} can engage in π-bonding to oxygen, thereby involving all three 2p orbitals on each oxygen ion in bonding. In contrast, π-bonding to oxygen is not a factor for a main group ion like Sb^{5+}. In the absence of π-bonding the geometry of the cubic perovskite structure enables only one of the three 2p orbitals on oxygen to covalently bond with Sb^{5+}. Consequently, while linear bonding is favorable for the M 5s−O $2p_x$ σ interaction, a deviation of the M−O−M angle from 180° allows for some σ bonding interaction between the *M* 5s orbital and the other two oxygen 2p orbitals (O $2p_y$ and O $2p_z$). This effect will be discussed in detail in the following section and the Discussion (see, for example, schemes 2, 3, and 4).

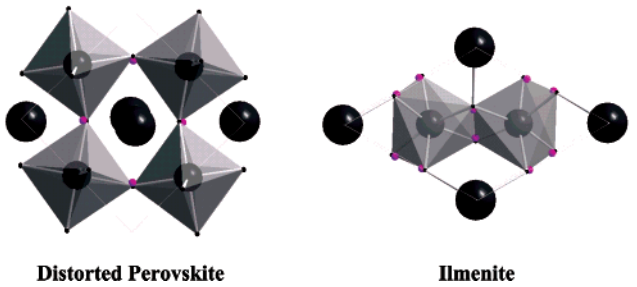

Figure 5. Polarization effects for $NaSbO_3$ as calculated by GULP, for the *Pnma* distorted perovskite structure, and the $R\bar{3}$ ilmenite structure. The location of the oxide core is shown with the small black spheres, while the center of gravity of the oxide shell is denoted with small pink spheres. The large gray spheres inside and outside the octahedra are Sb^{5+} and Na^{+} respectively.

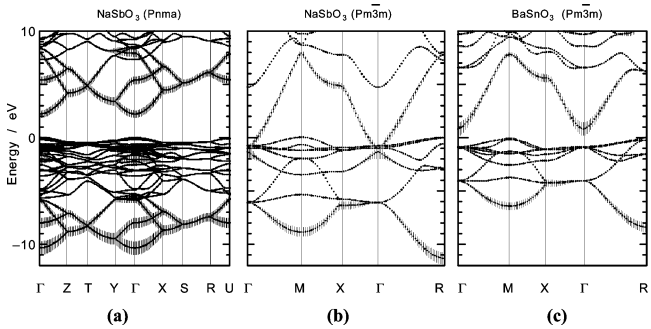

Figure 6. E-k diagram and Sb/Sn 5s-fatbands for (a) orthorhombic $NaSbO_3$ (*Pnma*), (b) cubic $NaSbO_3$ ($Pm\bar{3}m$), and (c) cubic $BaSnO_3$ ($Pm\bar{3}m$).

3.3. Electronic Band Structure Calculations. The electronic band structure (E−k diagram) obtained from LMTO calculations based on the distorted perovskite form of $NaSbO_3$ is shown in Figure 6a. The unit cell contains four formula units. The energy scale is defined so that the valence band (VB) maximum corresponds to zero energy. The conduction band (CB) minimum occurs at the Gamma (Γ) point, indicating that orthorhombic $NaSbO_3$ should be a semiconductor with direct band gap of 2.2 eV. This value underestimates the experimentally observed value of 3.4 eV, a phenomenon that is not unusual in cases where this method of calculating the electronic structure is applied to oxides. It has been suggested that the LMTO calculations tend to overestimate the width of the CB in oxides,[36,37] which is a possible reason for the underestimation of the band gap. The fatband depiction[38] shows that the Sb 5s

(36) Eng, H. W.; Barnes, P. W.; Auer, B.; Woodward, P. M. *J. Solid State Chem.* **2003**, *96*, 535.
(37) Mizoguchi, H.; Eng, H. W.; Woodward, P. M. *Inorg. Chem.* **2004**. In press.

orbitals make a strong contribution to the bottom four bands of the CB, as well as four filled bands that cover the energy range −5.5 to −10.3 eV. As there are only four Sb 5s orbitals in the unit cell, it becomes apparent that these two sets of bands arise from their antibonding and bonding interactions with oxygen (primarily O 2p). It is worth noting that the Sb 5s contribution to the bonding states is comparable to and perhaps a bit larger than its contribution to the antibonding states, reflecting the strong covalency of the Sb−O interaction, and indicating that the energy levels of the Sb 5s and O 2p orbitals are comparable, as shown in the MO diagram, **1**.

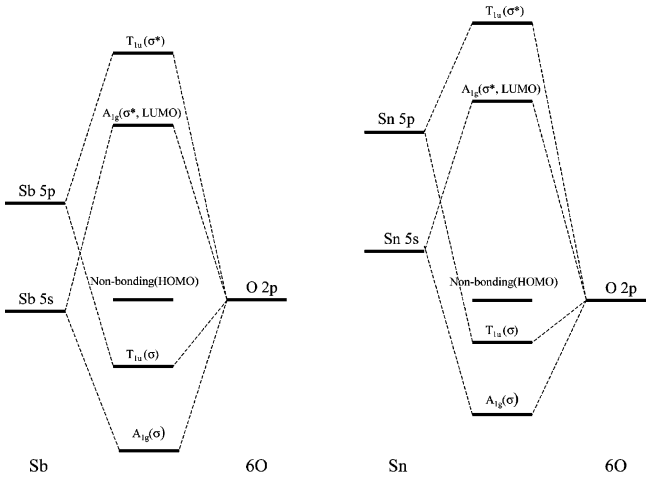

1

To better understand the electronic structure of this compound, it is instructive to consider what the electronic structure of $NaSbO_3$ would be if it adopted the cubic perovskite structure rather than the distorted $GdFeO_3$ structure. Figure 6b shows the electronic band structure calculated with the hypothetical cubic perovskite structure obtained from the CASTEP geometry optimization described in section 3.2. The change from orthorhombic to cubic causes the CB width to increase to the point where it overlaps the top of the valence band, resulting in a change from a semiconducting electronic structure to that of a metal, as shown in Figure 6b. As the unit cell now contains only one formula unit, the Sb 5s orbital contribution is concentrated primarily in two bands, corresponding to bonding and antibonding interactions with oxygen. The band structure of cubic $NaSbO_3$ shows good agreement with the electronic structure calculated by Singh et al.[39] for the hypothetical cubic perovskite $BaSbO_3$, despite the change in the antimony oxidation state. Given the fact that it has already been shown that LMTO calculations underestimate the band gap of orthorhombic $NaSbO_3$ by ∼1.2 eV, it is rational to expect that a similar shortcoming may be inherent to the calculated band structure of $NaSbO_3$ in the cubic perovskite structure. Therefore, it is likely that the cubic structure would not be metallic, but rather a semiconductor.

To analyze the collapse of the band gap in the hypothetical cubic (perovskite) form of $NaSbO_3$, consider the electronic structure for the semiconducting cubic perovskite $BaSnO_3$, shown in Figure 6c. Experimentally this compound is known to be a semiconductor with a band gap of 3.1 eV,[37] whereas the calculated band gap is only 0.9 eV. This result further illustrates the tendency of the LMTO calculations to underestimate band gaps in oxides. Nonetheless, the basic features of the band structure are similar to those of $NaSbO_3$ ($Pm\bar{3}m$), without the complication of the conduction band dipping into the valence band. Its electronic structure has been analyzed in some detail in a recently submitted publication,[37] but some of the salient features are highlighted here for understanding. The top of the valence band has primarily O 2p nonbonding character, but there is a small amount of antibonding O 2p−O 2p interaction that gives rise to slight dispersion at the top of the valence band. The lowest-energy band in the conduction band originates primarily from the Sn 5s−O 2p σ^* interaction. The representative orbital interactions are shown in one-dimension in **2**. At the X-, M-, and R-points the energy of the conduction band is high due to the strong antibonding interaction between the Sn 5s and O 2p orbitals. On the other hand, translational symmetry prevents mixing of the two states at the Γ-point; consequently, the bottom of the conduction band is predominantly Sn 5s nonbonding. This unusual feature of the cubic perovskite structure has been called superdegeneracy by Hughbanks.[40] In practice there is some antibonding Sn 5s−O 2s character. It is important to note that two of the three oxygen 2p orbitals (O $2p_y$, O $2p_z$) are forbidden by symmetry from taking part in the σ-bonding interaction with Sn. These orbitals comprise the essentially nonbonding lone pair states that dominate the electronic DOS at the top of the valence band.

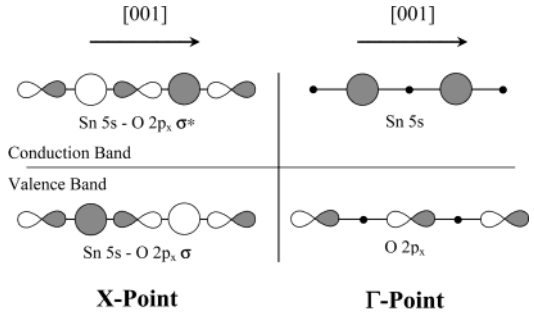

2

How does the situation change upon going from $BaSnO_3$ to $NaSbO_3$? First of all, the Sb^{5+} cation is more electronegative than Sn^{4+}, which lowers the energy level of the Sb 5s atomic orbital, as shown in **1**. The second effect of replacing Sn^{4+} with Sb^{5+} is a significant decrease in the *M*−O distance. It is expected that this decrease is larger than the orbital contraction that occurs upon moving from Sn^{4+} to Sb^{5+}, so that the net effect is an increase in the orbital overlap and the covalency of the *M*−O bonds. The fact that cubic $NaSbO_3$ shows increased splitting of the bonding and antibonding states at the M- and R-points, with respect to $BaSnO_3$, leaves no doubt that the Sb−O bonds are more covalent than the Sn−O bonds. In a molecule or a

(38) "Fatbands" are used to highlight the individual orbital contributions to each band. The width of the hatching corresponds to the amount of contribution of a particular atomic orbital to the band in question. Fatbands are a useful tool to quantify the change in orbital contribution from band to band, and within a given band as one moves through reciprocal space.

(39) Singh, D. J.; Papaconstantopoulos, D. A.; Julien, J. P.; Cyrot-Lackmann, F. *Phys. Rev. B* **1991**, *44*, 9519.

(40) (a) Hughbanks, T. *J. Am. Chem. Soc.* **1985**, *107*, 6851. (b) Wheeler, R. A.; Whangbo, M.-H.; Hughbanks, T.; Hoffmann, R.; Burdett, J. K.; Albright, T. A. *J. Am. Chem. Soc.* **1986**, *108*, 2222.

solid where the octahedra are isolated from each other (i.e. an ordered perovskite such as Sr_2ScSbO_6), the increased electronegativity of the Sb^{5+} cation would be offset by the stronger antibonding interaction and the HOMO−LUMO gap (the band gap in a solid) would not necessarily be reduced. However, as described above, the translational symmetry of the cubic perovskite structure is such that the conduction band minimum (LUMO) is nonbonding rather than antibonding. Consequently, cubic $NaSbO_3$ would be expected to have a considerably smaller band gap and wider conduction band than $BaSnO_3$. This expectation is consistent with the calculations.

4. Discussion

Among AMO_3 oxides, where M is a cation that prefers octahedral coordination, the most stable crystal structure is dictated by the competition between ionic bonding (lattice energy) and covalent bonding (electronic energy). The covalent bonding can be further categorized into contributions from $M-O$ σ-bonding and $M-O$ π-bonding. Simple lattice energy calculations show that ionic forces favor the corner-sharing connectivity of the perovskite structure over the edge-sharing connectivity of the ilmenite structure, as expected from Pauling's rules. Upon introducing polarization effects, the stabilization of the perovskite structure, with respect to the ilmenite structure, is significantly diminished. As pointed out by Blasse, polarization and covalency are closely related but not identical concepts.[4] In some cases there is a reasonable correlation between bonding and polarization. For example, an anion coordinated to two cations will experience more favorable polarization and σ-bonding interactions as the $M-O-M$ angles distort from 180° toward 90°. On the other hand, there are many instances where polarization does not mimic covalency. Consider for example the linear $M-O-M$ linkages of the cubic perovskite structure. The linear geometry is optimal for M $(n-1)$d−O 2p π-bonding interactions, but it provides no polarization stabilization whatsoever. Clearly covalent interactions must be explicitly considered to be able to understand the structural preferences of these compounds.

Ionic forces cannot be used to explain the distinctly different crystal chemistry of $ASbO_3$ and $ABiO_3$ from that of $ANbO_3$ and $ATaO_3$. From a covalent bonding perspective the cubic perovskite structure is not a favorable structure type in cases where M is a main group cation, as is the case for Sb^{5+} and Bi^{5+}. This statement is based on the fact that in the absence of π-bonding only one of the three oxygen 2p orbitals can participate in bonding to M. The stability of an asymmetric arrangement of cations about the anion was pointed out by Blasse.[4] This idea and its link to covalency was also pointed out by Goodenough and Kafalas, who explicitly noted that covalent bonding at the anion should be stronger if different anionic orbitals are used for each cation−anion bond.[5] The unfavorable hybridization at oxygen can be improved by distorting the $M-O-M$ bonds away from the linear configuration. This effect is well-known in molecules containing two-coordinate oxygen. Consider for example the comparison between H_2O and ilmenite $NaSbO_3$. The oxygen in water forms two covalent bonds to hydrogen with an H−O−H angle of ~105°. The oxygen coordination is similar in the ilmenite form of $NaSbO_3$, where oxygen forms two strong covalent bonds to antimony with an Sb−O−Sb angle of ~100°. This bonding stabilization is clearly seen in the CASTEP (DFT) calculations; it is also approximated in the GULP calculations through the introduction of polarization effects. However, in $NaSbO_3$, unlike water, the ionic interactions between Na^+ and the SbO_3^- framework play an important role. Consequently, the most stable structure will represent a balance between ionic forces, which favor the corner-sharing connectivity of the perovskite structure, and σ-bonding effects, which favor the edge-sharing connectivity of the ilmenite structure. For less electronegative main group cations, such as Sn^{4+}, Ga^{3+} and Al^{3+}, ionic interactions stabilize the perovskite structure despite the unfavorable covalent bonding at oxygen. However, as the covalency of the M ns−O 2p σ-bonding increases (M = Sb^{5+}, Bi^{5+}, Se^{6+}, Te^{6+}) covalent bonding considerations become increasingly important, and the perovskite structure is destabilized.

Ordered perovskites are a bird of a different feather. The perovskite topology is favorable for 1:1 ordered perovskites, such as Sr_2FeSbO_6,[42] Sr_2ScSbO_6,[43] and Sr_2MgTeO_6,[44] provided the second octahedral cation does not form strong σ-bonds with oxygen. These compounds are stable because oxygen is only required to form one strong σ-bond with a neighboring cation. In such compounds octahedral tilting does not significantly change the $M-O$ interaction and ionic considerations favor the perovskite topology. However, the ordered perovskite structure will become less stable as the σ-bonding power of the second octahedral cation increases. As an illustration of this concept consider the structural preferences of $Na_2M'TeO_6$ (M' = Zr^{4+}, Ti^{4+}, Sn^{4+}, Ge^{4+}). If prepared at ambient pressure, Na_2ZrTeO_6 adopts the ordered perovskite structure,[45] while the other three compounds have structures closely related to that of ilmenite.[46] Clearly though, the balance between ilmenite and perovskite is a delicate one, because both Na_2SnTeO_6 and Na_2TiTeO_6 convert to ordered perovskites upon HPHT treatement at 7 GPa and 950 °C.[47] The strong driving force to avoid nearly linear Sb−O−Sb bonds is also responsible for the observation that $A_2M'SbO_6$ compounds generally possess a more highly ordered octahedral cation distribution than their $A_2M'NbO_6$ and $A_2M'TaO_6$ analogues.[48]

Another class of complex perovskites containing Sb^{5+} and Bi^{5+} are the body-centered cubic 3:1 ordered perovskites, such as $Ba_4NaSb_3O_{12}$[49] and $Ba_4NaBi_3O_{12}$.[50] These compounds contain linear Sb−O−Sb and Bi−O−Bi linkages in seeming contradiction to our assertion that this configuration is unstable. However, a closer look at the structure of $Ba_4NaSb_3O_{12}$[51] reveals that a distortion of a different type occurs. Na/Sb ordering creates two chemically distinct oxygen sites, O_{ap} (apical) and O_{eq} (equatorial). Ignoring the Ba−O contacts, O_{ap} is coordinated by one Sb cation and one Na cation, while O_{eq} is coordinated by two

(41) Vegas, A. *Acta Crystallogr., Sect. B* **1986**, *42*, 167.
(42) (a) Cussen, E. J.; Vente, J. F.; Battle, P. D.; Gibb, T. C. *J. Mater. Chem.* **1997**, *7*, 459. (b) Blasse, G. *J. Inorg. Nucl. Chem.* **1965**, *27*, 993. (c) Sleight, A. W.; Ward, R. *Inorg. Chem.* **1964**, *3*, 292.
(43) (a) Tauber A.; Tidrow S. C.; Finnegan R. D.; Wilber W. D. *Physica C* **1996**, *256*, 340. (b) Fesenko, E. G.; Filip'ev, V. S.; Kupriyanov, M. F.; Devlikanova, R. U.; Zhavoronko, G. P.; Ochirov, V. A. *Izv. Akad. Nauk SSSR, Neorg. Mater.* **1970**, *6*, 800.
(44) Bayer, G. J. *J. Am. Ceram. Soc.* **1963**, *46*, 604.
(45) Bayer, G. *Fortschr. Mineral.* **1969**, *46*, 41.
(46) Woodward, P. M.; Sleight, A. W.; Du, L.-S.; Grey, C. P. *J. Solid State Chem.* **1999**, *147*, 99.
(47) Park, J.-H.; Parise, J. B.; Woodward, P. M.; Lubomirsky, I.; Stafsudd, O. *J. Mater. Res.* **1999**, *14*, 3192.
(48) Woodward, P. M. Ph.D. Dissertation, Oregon State University, Corvallis, OR, 1997.
(49) Alonso, J. A.; Mzayek, E.; Rasines, I. *Mater. Res. Bull.* **1987**, *22*, 69.
(50) Subramanian, M. A. *J. Solid State Chem.* **1994**, *111*, 134.
(51) Reis, K. P.; Jacobson, A. J.; *Acta Crystallogr., Sect. C* **1993**, *49*, 1585.

Sb cations. The coordination environment at antimony is a compressed octahedron, with two short Sb−O_{ap} bonds (1.89 Å) and four long Sb−O_{eq} bonds (2.07 Å). $Ba_4NaSb_3O_{12}$ is an electrical insulator with a band gap of ∼3.8 eV, as measured by diffuse reflectance spectroscopy. Our analysis of the electronic structure shows that the O_{eq} 2p orbitals make no contribution at the conduction band minimum (located at the Γ-point) for the same reason that the conduction band minimum is Sn 5s nonbonding in the cubic perovskite $BaSnO_3$. On the other hand, the O_{ap} 2p orbitals contribute significantly to the lowest-energy conduction band states at all points in the Brillouin zone. Thus, to a reasonable approximation we can think of O_{ap} as a terminal oxygen and O_{eq} as a bridging oxygen. If we were to begin with an idealized structure where all of the Sb−O distances were equal, the actual structure could be realized from a second-order Jahn−Teller distortion about antimony that dramatically compresses the octahedra and lowers their symmetry from O_h to D_{4h}. This type of distortion is made possible by the large difference in electronegativity between Na^+ and Sb^{5+}/Bi^{5+}.

The comparison between the isostructural perovskites $NaSbO_3$ and $NaTaO_3$ is an interesting one. The Sb^{5+} ion has a slightly smaller crystal radius than Ta^{5+} (0.74 vs 0.78 Å),[35] giving $NaSbO_3$ a larger tolerance factor. The smaller size of Sb^{5+} is consistent with the observed octahedral bond distances in the two perovskites. The average Sb−O distance is 1.965 Å in $NaSbO_3$, while the average Ta−O distance is 1.978 Å in $NaTaO_3$. Consequently, one would expect a smaller octahedral tilting distortion in $NaSbO_3$. However, the *M*−O−*M* angles reveal the opposite trend. The Sb−O−Sb angles in $NaSbO_3$ are 154.2(6)° and 154.2(8)°, noticeably smaller than the corresponding Ta−O−Ta angles of 158.8° and 160.1°. Clearly the increased octahedral tilting in $NaSbO_3$ cannot be driven by the Na^+ cation. In fact, the sodium cation pays the price for the increased tilting by accepting an overbonded coordination environment, as can be seen from the Na^+ bond valence sums[14] of 0.99 in $NaTaO_3$ and 1.27 in $NaSbO_3$.[52] Ideally, the bond valence sum should be very close to the oxidation state of 1. The good agreement between the observed and expected bond valence sum for Na^+ in $NaTaO_3$ shows that the octahedral tilting distortion in this compound is driven by the desire to optimize the ionic interaction between the sodium cation and its surrounding oxide neighbors.

The overbonding of Na^+ in $NaSbO_3$ has two effects: it destabilizes the perovskite structure and limits the magnitude of the octahedral tilting distortion. As support for the former assertion, consider that the sodium bond valence sums in the Na*M*O_3 compounds in Table 1 all fall between 1.01 and 1.17, considerably closer to the ideal value of 1.00 than the BVS of 1.27 found for perovskite $NaSbO_3$. As support of the latter claim, it is instructive to consider the structure of TeO_3.[53] The topology of the TeO_3 structure is the same as the corner-sharing octahedral network of the perovskite structure. However, instead of adopting a cubic structure, as ReO_3 does, it undergoes a very large $a^-a^-a^-$ octahedral tilting distortion,[54] which produces a rhombohedral crystal structure (see Figure 1f). The Te−O−Te bond angles are 138°, revealing a considerably larger octahedral tilting distortion than that seen in $NaSbO_3$. This distortion must be driven by covalency as the cation−anion distances are essentially unchanged by the distortion, while the anion−anion and cation−cation distances both decrease in response to the tilting. Unlike the case of $NaSbO_3$ where Na−O repulsive interactions limit octahedral tilting beyond a certain point, there is no *A*-site cation to resist the octahedral tilting in TeO_3. The behavior of TeO_3 also suggests that σ-bonding covalency effects favor structures such as ilmenite and cubic-$KSbO_3$ because of their highly bent *M*−O−*M* bonds and not because of some intrinsic stability associated with edge-sharing octahedra, as suggested by Blasse.[4]

How can we understand the nature of the electronic distortion that leads to octahedral tilting in $NaSbO_3$ and TeO_3? Returning to the band structure of a cubic perovskite, such as $BaSnO_3$, we noted earlier that at the Γ-point the orbital character of both the valence band maximum and the conduction band minimum are nonbonding (neglecting the O 2s contribution). As we move away from the Γ-point in any direction, the conduction band character changes from *M* 5s nonbonding to *M* *n*s−O $2p_x$ σ-antibonding, and the band energy increases. At the same time one of the O 2p-based bands in the valence band changes from O 2p nonbonding to *M* *n*s−O $2p_x$ σ-bonding, and the energy of this band decreases. This overlap was shown in **2** for the change from the Γ-point to the X-point. Despite the favorable *M* *n*s−O $2p_x$ σ-bonding interaction, the O $2p_y$ and O $2p_z$ orbitals are oriented perpendicular to the *M*−O−*M* bonds and are of the incorrect symmetry to participate in σ-bonding to the octahedral cation. The octahedral tilting distortion changes the electronic structure in two important ways. First of all, the O $2p_y$ and O $2p_z$ orbitals start to take part in the chemical bonding with the *M* 5s orbitals in the zigzag bent chains of the orthorhombic structure, as shown in **3**. Consequently, the orbital overlap at the Γ point is no longer strictly nonbonding. The introduction of antibonding character into the conduction band states increases their energy, while at the same time corresponding valence band states are stabilized by the introduction of bonding character. As the conduction band states are empty and the valence band states are filled, the distortion leads to a net stabilization of the electronic energy. Thus, we see that this distortion can be classified as a second-order Jahn−Teller distortion. The antibonding interaction that comprises the bottom of the conduction band is shown in **4**. In this illustration the sodium ions have also been included, but their covalent interaction with oxygen will be much smaller than the Sb−O interaction. The net effect in both $NaSbO_3$ and TeO_3 is to increase the size of the optical band gap and to narrow the width of the conduction band. As with any second-order Jahn−Teller distortion the driving force will increase as the energy separation of the affected electronic states decreases. Thus, the driving force for the distortion should increase as the cation electronegativity increases: $Sn^{4+} < Sb^{5+} < Te^{6+}$.

The type of distortion described in the preceding paragraph is different from second-order Jahn−Teller distortions associated with cations, such as out-of-center distortions of d^0 cations (i.e. Ti^{4+} in $BaTiO_3$ and Nb^{5+} in $KNbO_3$) and lone-pair distortions of s^2p^0 cations (i.e. Pb^{2+} in PbO or Bi^{3+} in Bi_2WO_6) in that the distortion occurs so as to alter the coordination environment at the anion site rather than at the cation site. However, it is similar

(52) These Na^+ BVS have been calculated from the eight shortest Na−O distances.
(53) Loub, J. *Z. Anorg. Allg. Chem.* **1968**, *362*, 98.
(54) (a) Glazer, A. M. *Acta Crystallogr., Sect. B* **1972**, *28*, 3384. (b) Woodward, P. M. *Acta Crystallogr., Sect. B* **1997**, *53*, 32.

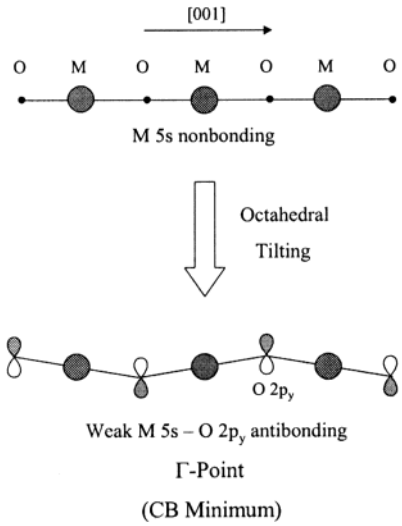

3

to the distortion seen in the β-cristobalite polymorph of SiO_2. That structure contains corner-connected SiO_4 tetrahedra, and through the years has often mistakenly been described as cubic (space group $Fd3m$) with linear Si−O−Si bonds. In reality β-cristobalite has a tetragonal crystal structure, and the Si−O− Si bond angle is closer to 147° than 180°.[55] The fact that anion-based second-order Jahn−Teller distortions are not readily recognized by chemists probably has less to do with the frequency with which they are observed and more to do with widespread adoption of Pauling's suggestion to consider extended ionic-covalent solids as built up from cation-centered polyhedra. There is no doubt that such an approach is a very useful one, but it does tend to obscure some aspects of structure and bonding if used to exclusion.

5. Conclusions

In conclusion, we have synthesized a new polymorph of $NaSbO_3$ with high-pressure−high-temperature synthesis techniques. The high-pressure form of $NaSbO_3$ was quenched back to ambient conditions where it was characterized. It adopts an orthorhombically distorted perovskite structure (space group = *Pnma*), isostructural with $CaTiO_3$, $GdFeO_3$, and $NaTaO_3$. It is a white insulator with an optical band gap of 3.4 eV. This compound is the first ternary perovskite prepared that contains Sb^{5+} on the octahedral site, and as such it provides considerable insight into structure−bonding relationships in main group metal oxides. The octahedral tilting distortion in this compound is larger than expected from ionic radii considerations. Analysis of the electronic structure shows that the octahedral tilting in this compound is driven by a second order Jahn−Teller distortion that can be traced back to strong Sb−O covalent bonding. The conflict that arises from the electronically driven octahedral tilting distortion and the repulsive Na−O interactions, which oppose excessive octahedral tilting, are responsible for destabilization of the perovskite form of $NaSbO_3$ under ambient conditions. Our analysis shows that M *n*s−O 2p covalency drives AMO_3 (M = Sb^{5+}, Bi^{5+}, Se^{6+}, Te^{6+}) compositions to adopt structures where the M−O−M angles are strongly distorted from linear. This feature is responsible for the stabilization of structures that contain edge-sharing octahedra in violation of Pauling's rules for understanding ionic crystal structures.

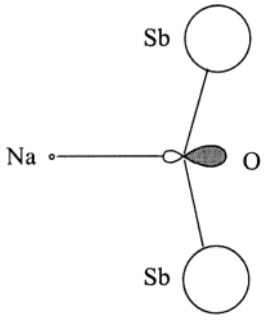

4

Acknowledgment. We thank Professor O. K. Andersen and Dr. O. Jepsen (Max Plank Institute, Stuttgart, Germany) for providing us with the LMTO codes and for support. We also thank Dr. J. D. Gale (Curtin University, Perth, Australia) for allowing us to use GULP. Research carried out at Ohio State was supported by the National Science Foundation Grant DMR-0094271. Research carried out at Stony Brook was supported by Grants NSF-DMR-0095633 and EAR-0125094.

JA038365H

(55) Hyde, B. G.; Andersson, S. *Inorganic Crystal Structures*; Wiley: New York, 1989; p 392.